VĚDECKÉ SPISY VYSOKÉHO UČENÍ TECHNICKÉHO V BRNĚ

Edice PhD Thesis, sv. 363

ISSN 1213-4198

Ing. Filip Lopour

Development and application of an UHV SPM microscope

Brno University of Technology
Faculty of Mechanical Engineering
Institute of Physical Engineering

Ing. Filip Lopour

Development and application of an UHV SPM microscope

Vývoj a aplikace mikroskopu UHV SPM

Short version of Ph.D. Thesis

Study field:	Physical and Materials Engineering
Supervisor:	prof. RNDr. Tomáš Šikola, CSc.
Opponents:	doc. RNDr. Pavel Sobotík, CSc. Ing. Vladimír Cháb, CSc. doc. RNDr. Jaroslav Pavlík, CSc.

Presentation date: January 25th, 2006

KEY WORDS:

atomic force microscopy, micro/nanostructures, local anodic oxidation, nanotechnology, scanning tunneling microscopy, tip induced nanostructures, scanning electron microscopy, low vacuum secondary electron detector

KLÍČOVÁ SLOVA:

mikroskopie atomárních sil, mikro/nanostruktury, lokální anodická oxidace, nanotechnologie, rastrovací tunelová mikroskopie, nanostruktury vytvořené hrotem, rastrovací elektronová mikroskopie, nízkovakuový detektor sekundárních elektronů

Full version of the Ph.D. Thesis is deposited at the Department of Science and Research, Faculty of Mechanical Engineering, Brno University of Technology, Technická 2, 616 69 Brno, Czech Republic.

Disertační práce je uložena na oddělení vědy a výzkumu FSI VUT v Brně, Technická 2, 616 69 Brno.

ISBN 80-214-3139-3
ISSN 1213-4198

TABLE OF CONTENTS

1 INTRODUCTION

Scanning probe microscopy (SPM) has undergone a vast development during the last two decades. At present, several thousands of papers dealing both with this technique and relevant applications are published yearly. Its fundamentals have been laid by the invention of scanning tunneling microscopy (STM) by Binning and Rohrer [1] and later by its extension to observations of nonconductive surfaces [2], being known as atomic force microscopy (AFM).

In the Institute of Physical Engineering at Brno University of Technology, an ultra-high-vacuum (UHV) compatible instrument for scanning tunneling microscopy and atomic force microscopy (STM/AFM) has been developed in close cooperation with TESCAN, s.r.o. [3]. These microscopic techniques have helped us to investigate the mechanisms of thin film growth, surface/thin film morphology and microstructures produced by ion beam technology. Furthermore, the modified STM/AFM instrument was used for fabrication of micro and nanostructures.

In Section 2 a general overview of AFM technique and a design description of the STM/AFM instrument that has been built in our institute are given. This section deals with some particular aspects of instrument design (i.e. design of an optical detection unit and calibration of a piezoscanner) and demonstrates the ability of the instrument to obtain atomically resolved images. In Section 3 the examples of application of the AFM technique to evaluate thin film deposition and surface modification by ion beam are presented. Section 4 introduces a technique of local anodic oxidation carried out by AFM that was used for fabrication of micro- and nanostructures. The software and hardware modifications of the AFM instrument essential for this technique and results of the experiments are described there.

Section 5 summarises the results of the author's contribution to a project of high temperature ultra-high vacuum scanning tunneling microscopy at a partner's university abroad. This project was dealing with an atomic resolution imaging on Si(111) and with tip induced fabrication of the nanostructures at its surface. Last part of the thesis aims to the field of scanning electron microscopy - SEM. It overviews the development of the novel secondary electron detector for low vacuum SEM that have been done in the company TESCAN, s.r.o. and resulted in an international patent application.

2 SCANNING PROBE MICROSCOPE - DESIGN AND OPERATION

2.1 PRINCIPLES OF THE OPERATION

Contrary to very well known STM, where the tunneling current through a sharp tip as a function of the tip-to-surface distance is measured, AFM is based on the detection of forces between an observed sample surface and a sharp tip located at the end of a cantilever. The commercially available silicon or silicon nitride cantilevers are generally of a triangular shape with a typical length of 100 – 300 μm [4]. The diameter of the tip is in the order of tens of nanometres. For high resolution applications a specially sharpened tips with diameters close to 5 nm are used.

If the cantilever is in a direct contact with a surface, the repulsive forces resulting from quantum mechanical principles prevail, and we speak about the contact mode. The contact mode may lead to significant damages of the analysed surface due to scratches, defects and reconstruction caused by the tip.

The noncontact mode of AFM, where the tip is not in a direct contact with a surface, significantly reduces this problem. The technique belongs to less destructive methods and is particularly suitable for surface analysis of soft samples. Quite recently, the true atomic resolution on selected surfaces (e.g. Si, GaAs, InP, NaCl) by means of the noncontact AFM has been demonstrated. In this method, the tip interacts with surface atoms mainly by means of long-range attractive van der Waals forces and likely by an onset of covalent bonds. The principle of the measurements of surface topography is based on changes in the effective resonance frequency of the oscillating cantilever (vibrations of that are excited by an external generator via a piezoceramic element) with a tip-to-surface distance [5].

The forces acting on a cantilever in AFM are determined from the bending of the cantilever. The most sensitive and thus most frequent detection method of the cantilever bending is the optical displacement method. In this method, depending on the bending of the cantilever, the laser beam after its reflection from the cantilever surface is deflected into different parts of the position sensitive photodiode (PSPD). The electrical signal from PSPD, proportional to a beam deflection, is processed via an electronic system identical with STM electronics and might be used as a pilot signal for the feedback control of a tip-to-surface distance by a piezoscanner.

2.2 DESIGN OF THE MICROSCOPE

The UHV SPM microscope, which has been developed at the Institute of Physical Engineering, has a vertical configuration and is mounted on a UHV CF flange DN 150. The base plate of the SPM microscope is suspended on four springs to reduce the transfer of external vibrations into the microscope. The resonance frequency of the suspended system is approximately 1.8 Hz. As generally the damping of resonance vibrations of the base plate is under UHV conditions extremely low, it is enhanced by a magnetic damping system formed by a set of permanent magnets and copper plates (eddy current damping effect).

Top view of the SPM apparatus is shown in Fig. 1. The samples or probes are mounted on prismatic holders that enable their easy replacement by means of vacuum tweezers. Alternatively, a piezoceramic plate is placed between the cantilever and the holder in order to generate forced oscillations of the cantilever. In the noncontact AFM mode the plate is supplied by alternating voltage (sinusoidal waveform) from a generator. During the image recording the probe is in fixed position and sample is moved above it by means of a 3-axis piezoceramic scanner providing a maximum field of view of 6x6 μm^2 in the x-y direction and ±2 μm in the z direction. A coarse approach of a sample to the tip is realized by a linear inchworm motor. A single step of the linear motor is very fine and can be adjusted in the range of 0.2 to 1 µm. However, by repeating the single steps a long distance movement as much as 15 mm can be realized.

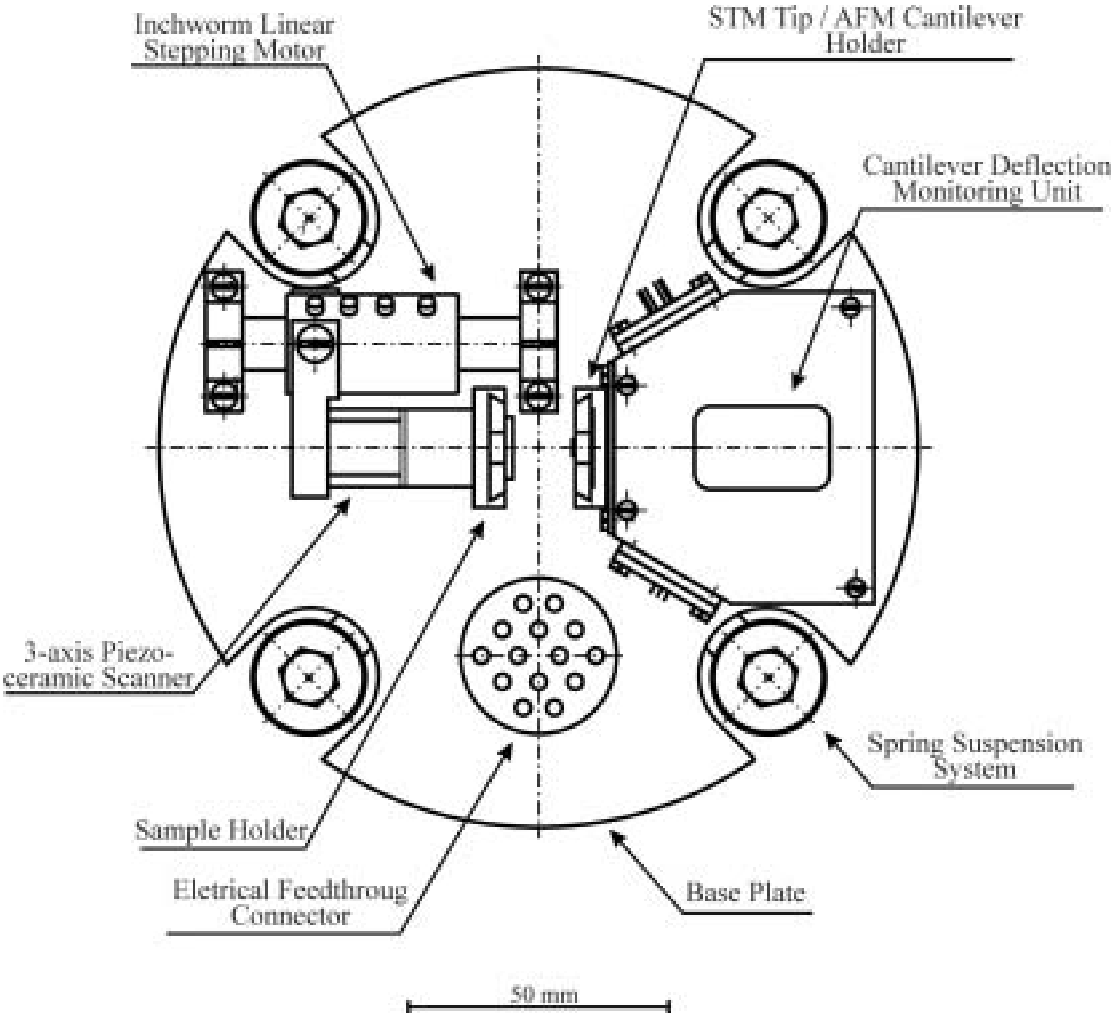

Fig. 1: UHV SPM apparatus - top view.

The control unit of the microscope and relevant software have been modified from the older version produced by TESCAN, s.r.o. for STM microscopes. Additional details of the microscope design have been published in [6] and, partially, in [7].

2.3 NEW OPTICAL DETECTION UNIT

As a part of this project a new optical detection unit has been designed, built and implemented. The detection unit fixed to the base plate consists of a laser diode, cantilever mounted on its holder, 4-segment position sensitive photodiode (PSPD) and two adjustable mirrors, see Fig. 2. The mirrors provide fine aligning of the laser beam at the cantilever end and at the PSPD centre. Additionally, they prolong the total optical path length thus improving the resolution of the detection system [6].

In order to provide the remote movement control of the mirrors, the special attenuators have been developed according to [8]. The rotation of the ball with the fixed mirror is realized by inertial piezoceramic motors, the method being called the slip-stick motion. The two shear piezoceramic plates are first driven by slow ramping input voltage to move in one direction. The steel ball follows their movement because of friction - the “stick” part of the motion. Then the plates are forced to retract quickly to their original position by a sudden drop of the voltage. Because of the inertia principle the friction force is exceeded and the ball does not follow the plates - the “slip” part of the motion. Repeating the single steps the total angular movement of several degrees is achieved.

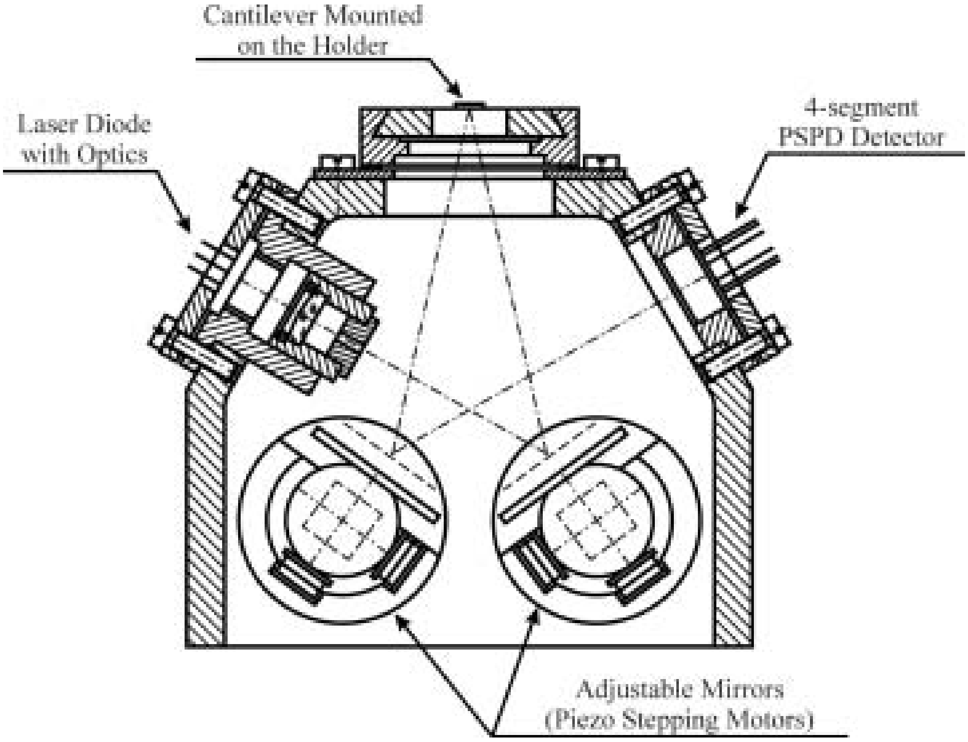

Fig. 2: New optical detection unit of SPM microscope.

The mirror attenuators designed consist of the stainless steel bedding, the steel ball, the mirrors, the magnet and the shear plates. The shear plates 5x5 mm size and 0.5 mm thickness are attached to the attenuator bedding by the conductive epoxy glue. There are 2 of them per one axis of rotation, i.e. 6 plates per one attenuator. The piezoceramic material PIC 131 [9] was selected due to its high mechanical Q-factor resulting in a fast response to the driving voltage.

The driving pulses for the piezoceramic plates were generated by a high power supply from the original Tescan control unit. The shape of the pulses and their frequency could be optimized in order to obtain a reasonable speed of the mirror rotation and the movement reliability. Adjusting the friction force can be done by moving the magnet in the mirror bedding. After the parameters were optimized the attenuators worked well under atmospheric conditions. However, during the tests under vacuum conditions the mirrors got stuck. It can be explained by a lack of humidity in vacuum and consequent effect of sticking the parts to each other. It was suggested that the power supply used is too “slow” to ramp the voltage at the shear plates fast enough to exceed “sticking force”. Currently, a new high voltage pulse supply is being developed to overcome this problem and preliminary results show a significant improvement in the mirror attenuators reliability.

2.4 CALIBRATION OF THE PIEZOSCANNER

When using the scanning probe microscope for estimating the real dimensions of surface features there is always a question how precisely the dimensions are measured, i.e. how accurate are the movements of the x-y-z piezoscanner. It is possible to calculate the range of this motion from physical constants of the piezoceramic. The piezo elongation is proportional to the applied voltage (electrical field), ceramic dimensions and the piezo strain coefficients [9]. However, the coefficients are guaranteed by a producer with a very low precision in order of ±10%. Further the error might be enhanced from tolerances of ceramic dimensions, electrode shape and way of fixing the piezoscanner to the metal parts. The most feasible way how to avoid the complicated analyzes of all these influences is a calibration by using the special sample of the known and guaranteed dimensions.

A nickel cross grating has been used for the calibration of the x-y scanning range of the piezoscanner. The grating has been made by the method of the interferential image of four laser beams (holographic technique) [10]. Although the grating parameter is precisely given by the wavelength of the laser and by the exposure geometry it was measured and confirmed to be 836nm by means of an optical diffraction method with the precision better then 0.05%. An image of the grating was taken in the AFM contact mode and the measured dimensions were used for the instrument recalibration.

For the calibration of the piezoscanner movement in the z-axis a sample with the lines of thermally oxidized silicon was used. It has been created by the electron-beam-lithography patterning and subsequent etching of the oxide layer. The SiO_2-lines height of 158nm was measured by a profilometer the precision of which is guaranteed to be within ±1% when using a standard for its calibration.

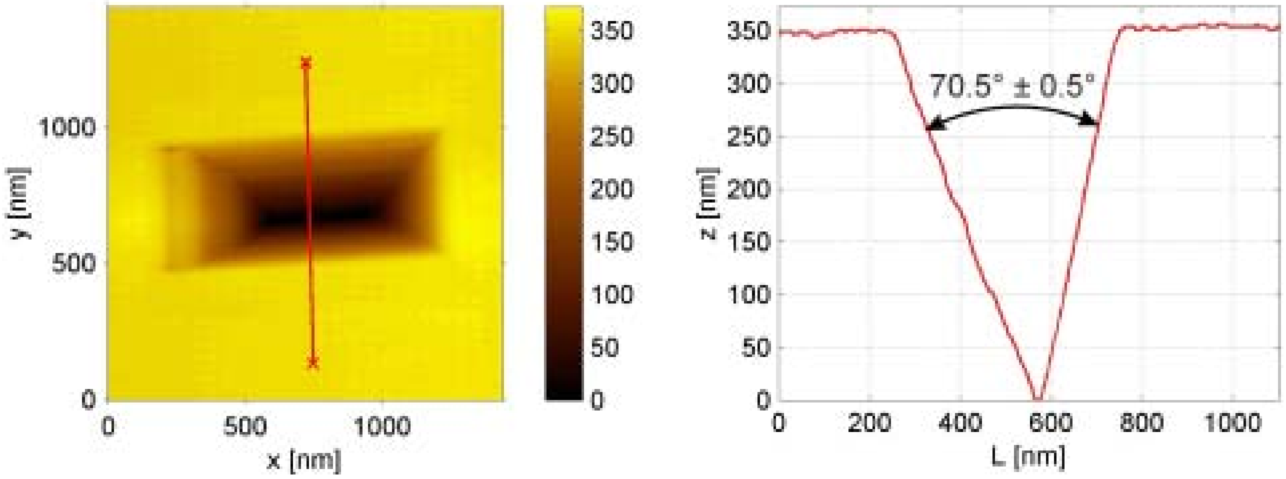

Fig. 3: Calibration verification by the angle between two Si(111) atomic planes.

The both x-y and z calibrations can be verified (cross checked) by the measurement of known angle at a sample surface. Such sample had been produced by an anisotropical etching of a single crystal Si(100) through a mask of SiO_2, Fig. 3. The side walls of the pyramidal shape pit are formed by the atomic planes of (111) direction. The angle of 70.5° between the walls is very precisely given by crystallography of silicon. When the piezoscanner is correctly calibrated in both x-y and z directions the measured angle must be found in a reasonable agreement with the real sample geometry. The measured angle values fell within less then ±1% error interval of the correct value. Further details on the technology of the samples preparation are given in [10].

2.5 ATOMIC RESOLUTION WITH STM

In order to verify a lateral and vertical resolution of the instrument a sample of highly oriented pyrolytic graphite (HOPG) was imaged by the technique of scanning tunneling microscopy (STM).

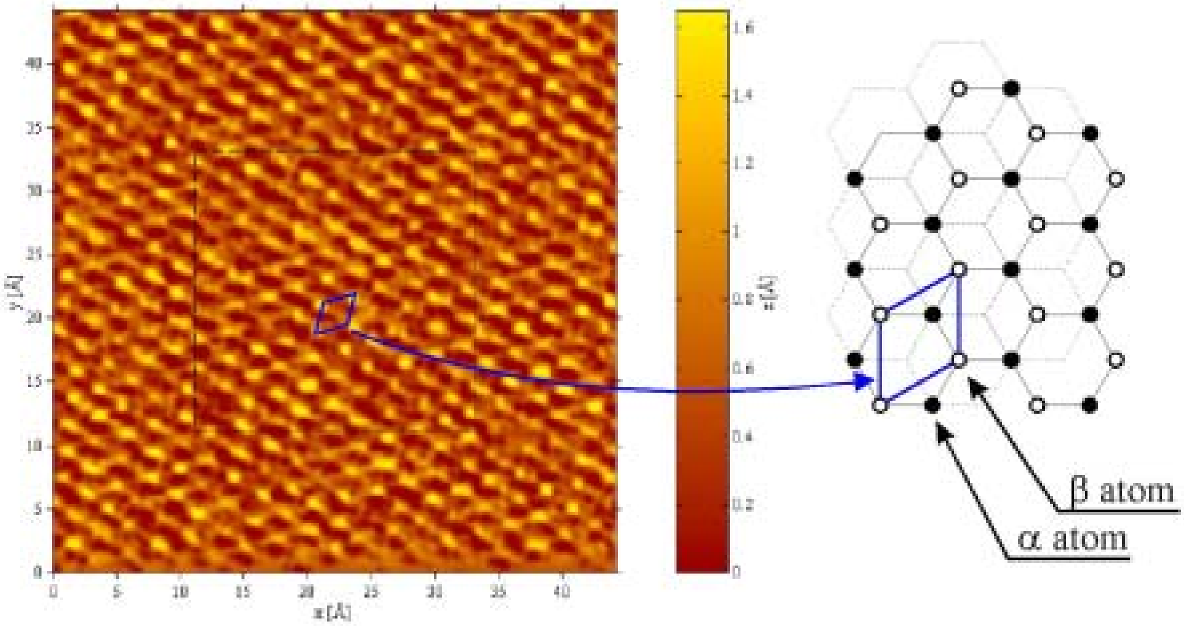

Fig. 4: STM constant-current-mode image of HOPG and the graphite structure.

Figure 4 shows the STM image recorded in the constant current mode at the sample bias 0.2 V and the tunneling current 0.5 nA under atmospheric conditions. The corresponding surface atomic structure of graphite is schematically shown on the right. Only β atoms, i.e. the atoms that have no direct neighbors in the in adjacent atomic plane below (the adjacent plane structure is marked in dashed lines), are visible in the STM image. This is due to the graphite crystal structure where the highest occupied and the lowest unoccupied electron surface states are centered at the β atom sites, therefore the tunneling current flows preferentially to the sites, independent of the sample bias polarity. This gives the evidence that the STM does not always show the pure topographic image of the surface; however, it is strongly influenced by a local electron density of states [12].

Despite of the fact that the STM image (Fig. 4) shows some imperfections caused by the electronic and environmental noise, the individual β atoms separated by the distance of 2.46 Å can be clearly distinguished. This confirms the capability of our instrument for the atomic resolution imaging.

3 AFM STUDIES OF SURFACES UNDER ATMOSPHERIC CONDITIONS

Our group at the Institute of Physical Engineering has been particularly interested in ion beam techniques. An apparatus for ion beam assisted deposition (IBAD) was designed and built in the Laboratory of Surfaces and Thin Films [13]. It has been used for deposition of thin films and modification of solid surfaces. Due to its ability of high resolution and real 3D imaging the AFM is particularly suitable for the studies of surface morphology at the micro/nanometre scale. In this section two examples of application of AFM are presented.

3.1 SURFACE ROUGHNESS MEASUREMENTS

For the study a series of samples of TiN and ZrN thin films was prepared by the IBAD technique. The apparatus consists of two broad beam Kaufman ion sources. The film is deposited on a silicon substrate by sputtering of a pure metallic target (Ti or Zr) by a primary ion beam (Ar^+, energy 600eV). Simultaneously, the deposited film is modified with a secondary ion beam, in this case N_2^+. The energy of secondary ion beam was varied from 0 to 400 eV.

After the deposition in the high vacuum apparatus the samples were inserted into the AFM instrument and imaged in the contact mode. In these measurements small fields of view and high vertical magnifications must be used as the surface of deposited films is very smooth. The root mean square (RMS) deviations of the measured vertical corrugations of deposited films at a field of view of 300 x 300 nm^2 were below 1 nm for any applied assisting ion energies.

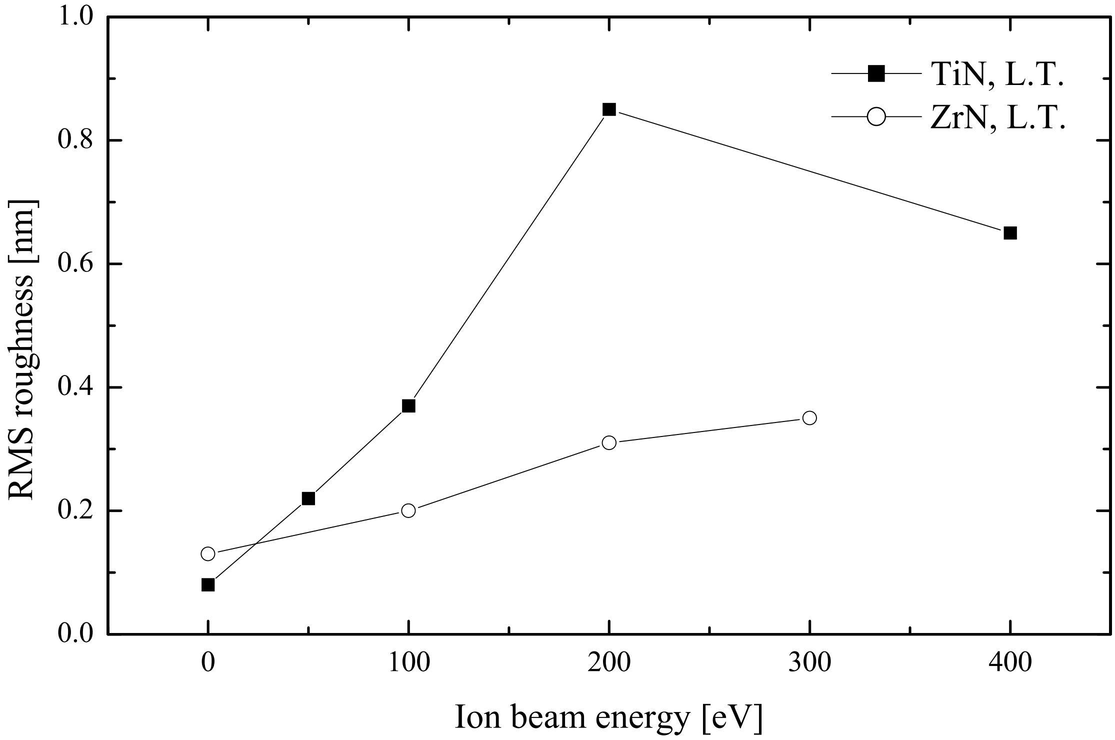

Fig. 5: RMS roughness as a function of the assisting ion beam energy.

The dependence of RMS roughness on the assisting ion beam energy is shown in Fig. 5. Approximately a linear dependence has been observed for the both nitrides;

however, the slope of a curve strongly depends on the material deposited. The decrease in RMS for the last point of TiN curve can be explained by resputtering process (the rate of deposition is lowered by the sputtering caused by the energetic assisting ion beam) [13].

3.2 ETCHING OF MICROSTRUCTURES

Low energy ion beams (E < 10 keV) have been frequently used for the etching of micron/sub-micron patterns where a high anisotropy of the etching process is required. In this section the etching ability of low energy argon ions to produce microstructures in Si and Ag substrates is demonstrated.

The main purpose of this study was to verify the ability of inert ion beams to etch microstructure patterns into silicon or metallic substrates. All experiments on the etching of microstructures were carried out in the IBAD apparatus described above. For etching only the primary ion beam source with a grid diameter of 150 mm was used (providing a beam diameter of about 50mm at the sample). To find proper conditions for the etching, the energy of the argon ion beam was varied from 400 eV to 1000 eV, which resulted in a variable ion current density at the target (within an order of 0.1 mA/cm^2), and different angles of ion beam incidence were applied. The morphology of etched patterns and modified surfaces was investigated by AFM under atmospheric conditions in the contact mode.

In our study four-sector grids with a series of parallel-line patterns in each sector were etched. The square-like sectors (2 x 2 mm) were different from each other in orientation of the individual line series. The grids with dimensions and periodicity of the line patterns similar to those used in optical grids were of particular interest. The patterned silicon and metal substrates might be used as reflection optical grids or as masters for casting grid patterns into plastic materials. The masks for etching of these grids were made of polymethylmethacrylate (PMMA) resist deposited on Si substrates or on Ag thin films on Si substrates by a spin coating technique. The patterns were drawn into 200 nm thin resist by electron beam lithography. The lateral periodicity of the lines was 1.3 μm and their width was 650 nm.

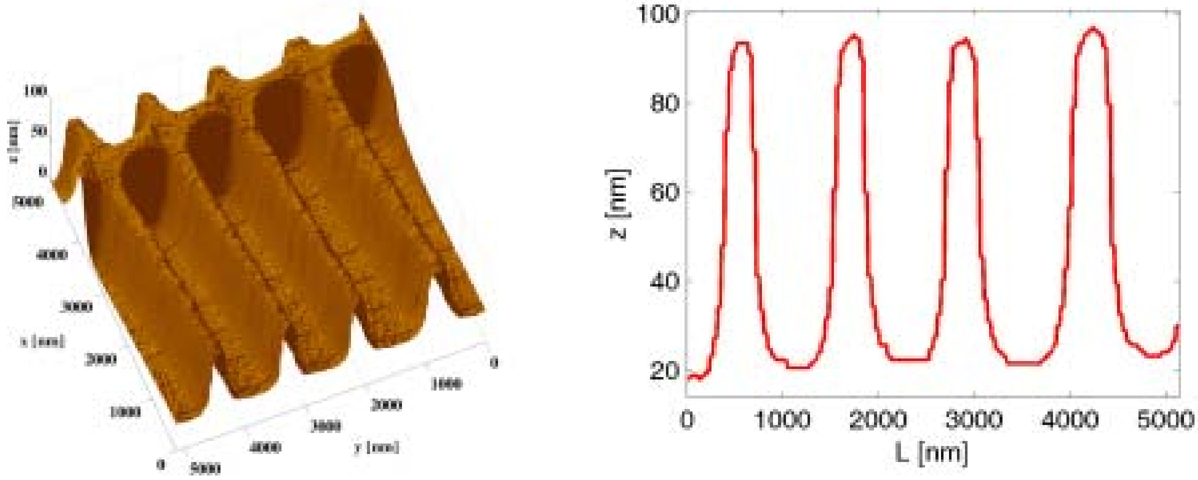

Fig. 6: AFM image of the Si pattern etched by a 600eV-Ar-ion beam under normal incidence, etching time 2:40 min.

In Fig. 6 a detailed AFM view of the patterns etched by a 600 eV-argon-ion beam under normal incidence into the Si substrate for 2:40 minutes is shown. The ion energy of 600 eV was kept in all etching experiments as a suitable compromise value ensuring reasonable etching rates at good protective properties of the resist. The 3D picture on the left shows pattern lines with smooth margins, the right figure shows a cross profile of the etched patterns. The profile is sharply featured with relatively flat tops and with a height of patterns close to 70 nm. Higher etching times (e.g. 3:40 minutes) led to over-etching of structures resulted in narrow profiles and sharp tops of the patterns. The grids etched by ion beams under an angle of 70° (from the Si surface) for 2:15 minutes had tilted profiles of a similar quality as those etched under normal incidence of the ion beam and the height was 90 nm. This was the highest value achieved by argon ion beams for good-quality patterns in silicon.

The only way how to increase the height of patterns was to use substrate materials with higher etching rates than that valid for silicon. As silver has approximately four times higher etching rate than silicon (200 nm/min for $j_i = 1$ mA/cm^2 at 500 eV), Ag thin films deposited on Si substrates were used for patterning. The results of etching experiments confirmed these expectations. For normal ion incidence the well shaped profiles with a pattern height of approximately 250 nm were obtained for an etching time of 1:50 min. This work was in more detail presented in [14].

4 APPLICATION OF AFM IN FABRICATION OF MICRO/NANOSTRUCTURES

Atomic force microscopy has been used for a study of surfaces of solids at the nanometre scale. Quite recently, AFM microscopes have also become laboratory tools for fabrication of various nanostructures and micro/nano-devices. In one of these technologies, the local anodic oxidation of non-noble metallic and semiconductor surfaces is carried out by a tip electrically biased by a negative potential towards the surface [15]. Contrary to STM, AFM is able to monitor the nonconductive nanostructures by the same tip after they have been fabricated.

In the technique of local anodic oxidation the oxides grow on a chemically reactive surface by local application of electric field. Highly localized and strong electric field (~10^6 V/mm) is created between a sample surface (anode) and a sharp conductive AFM tip (cathode) even when they are biased to a voltage only in an order of several volts. Water naturally absorbed at the surface under atmospheric conditions serves as an electrolyte and dissociates into OH- and O_2- or O- ions. Ions start the process of formation of oxides at the surface and, furthermore, due to the electric-field-induced diffusion the oxides grow underneath as well.

We have been concerned in nano-patterning of titanium thin films when the oxide layers are formed by a mixture of TiO and TiO_2. Due to the lower density, the oxidized material protrudes above the surface and therefore, oxide patterns are directly detectable by monitoring the surface morphology using AFM without additional etching.

4.1 INSTRUMENTATION AND SAMPLE PREPARATION

All experiments were done with the home-built SPM instrument. In order to extend the microscope ability to fabrication of nanostructures the original software was modified to accommodate the routines for defined under a specific tip-sample voltage. The following options have been added to the software:

- Line, square and pattern tip motion under a controlled tip-sample voltage.
- Setting of the writing speed between 1 to 2000nm/s.
- Pattern layout can be programmed by a text file defining the vectors of moving the tip, voltage applied to the tip and the writing speed. The voltage and speed can be assigned for each vector independently.

The local anodic oxidation of Ti films was carried out in the contact mode using conductive tips made of silicon covered by a 25 nm layer of W_2C, MicroMash CSC11/W2C A [4]. The tip radius specified by the producer was < 35 nm, its specific resistivity was below 50 μΩ cm. The same tip was used for consequent monitoring of the fabricated oxide structures.

Titanium films investigated and processed by AFM were prepared in an ion-beam-assisted deposition (IBAD) apparatus [13]. The thin films were deposited by sputtering titanium targets (purity 99.95%) using Ar^+ ion beam (600 eV). The thickness of the films used in the experiments ranged from 5 to 50nm. As substrates both Si(100) and Si covered with a thermal SiO_2 (240nm) film were used.

In the case that pattering of the film was required the substrate was covered by an electron positive resist (PMMA) and the pattern was exposed in the resist by the means of electron beam lithography. The exposed parts of the resist were removed by a solvent. After the deposition of a Ti film the pattern was developed by a conventional lift-off technique.

4.2 RESULTS AND DISCUSSION

In order to verify the ability of writing a defined oxide structures and find optimal conditions for nanostructure manufacturing the test patterns were made. First, a series of nanowires was made at different conditions.

Figure 7 shows a series of oxide nanowires fabricated on a Ti film (thickness 50 nm) for a set of distinct tip-sample voltages (6 – 9 V) at one constant writing speed $v = 100$ nm/s. From the profile cross section on the right it is obvious that the height of the lines grows with the applied voltage. To quantify the height and half- width of the oxide lines the parameters were measured and plotted as a function of voltage (Fig. 8). From the graph follows that the height of the lines grows linearly with the voltage and the dependence found by linear regression is $h = -3.80 + 1.44\ U$, where U is the tip-sample voltage. The linear dependence is in a good agreement with the results published in [16].

The theoretical threshold voltage (i.e. minimum electric field necessary to start the oxidation) calculated from the equation is 2.6V. This is in contradiction with the value observed in Fig. 7 showing that no oxidation process occurs at 5V and below. It suggests that the process is not linear in the vicinity of its threshold value.

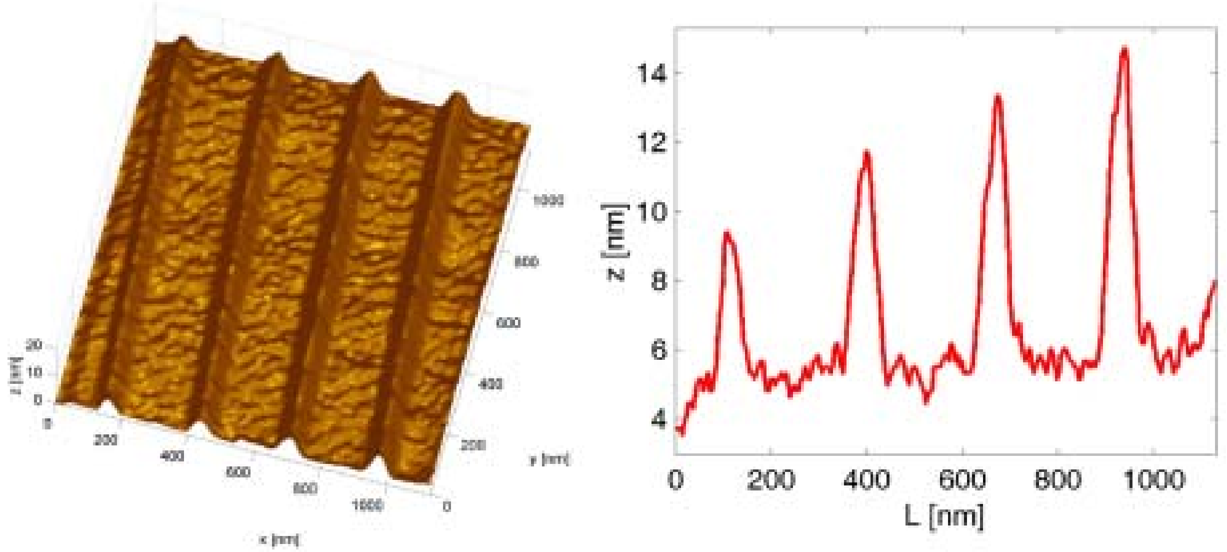

Fig. 7: A series of oxide nanowires fabricated on a Ti film made at a set of distinct tip-sample voltages (6 – 9 V) at a constant writing speed v = 100 nm/s.

Similar series of oxide lines was made for a fixed voltage of 6V and distinct writing speeds ranging from 20 to 100 nm/s. In this case a thinner Ti film 5 nm was used. The dependence of the height and half-width on a writing speed at a constant tip-sample voltage was plotted. It was found that the height of the oxide lines falls linearly with the speed v, which can be expressed by the equation $h = 4.41 - 1.51v$ (v is in nm/s). The line half-width does not decrease linearly over the studied interval of writing speeds.

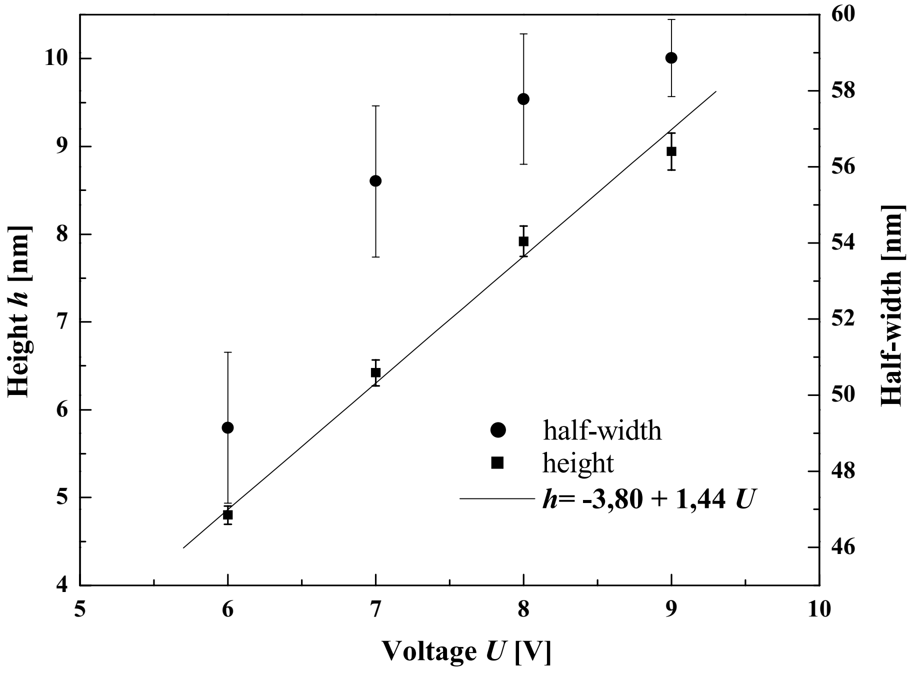

Fig. 8: Height and half-width of the oxide lines as a function of voltage.

Comparing the heights of the lines which were made under identical conditions ($U = 6$ V, $v = 100$ nm/s) one finds that the height of the first is significantly bigger (4.7 nm) than that in second case (< 1.4 nm). The distinct values of the line dimensional characteristics result from different thicknesses of Ti films used for oxidation. In case of 8 nm thick film, the oxide layer expanded throughout the whole film thickness until it reached the SiO_2 substrate where the process was stopped. On the contrary in case of 50nm film the process is stopped at a maximum depth to which oxygen can diffuse. This depth seems to be approximately three times larger than in the case of the of 8-nm thin film. If the film of a known thickness is completely oxidized through to a substrate, the ration of volumes before and after Ti oxidation can be calculated. From this ratio the chemical nature of oxides can be estimated [16]. In this way it was found that TiO is the prevailing form of the oxide type in the lines and TiO_2 content is practically negligible.

Local anodic oxidation might be used for a study of quantum effects in nanostructures (e.g. quantum conductivity effects, Coulomb blockade etc.) and for experiments in fabrication of nano-devices, e.g. single electron transistors (SETs) working at room temperature [17]. In Fig. 9 a detail of the structure for studies of quantum conductivity effects is demonstrated. The detail shows a section of 1.5 µm wide Ti conduction line. The Ti line was locally oxidized step by step from both sides by scanning an AFM tip in adjacent lines/squares along the Ti wire. In this way it was possible to make a narrow non-oxidized gap between two oxide areas. As the thickness of the Ti film was 8 nm only, the film was fully oxidized to the SiO_2 substrate.

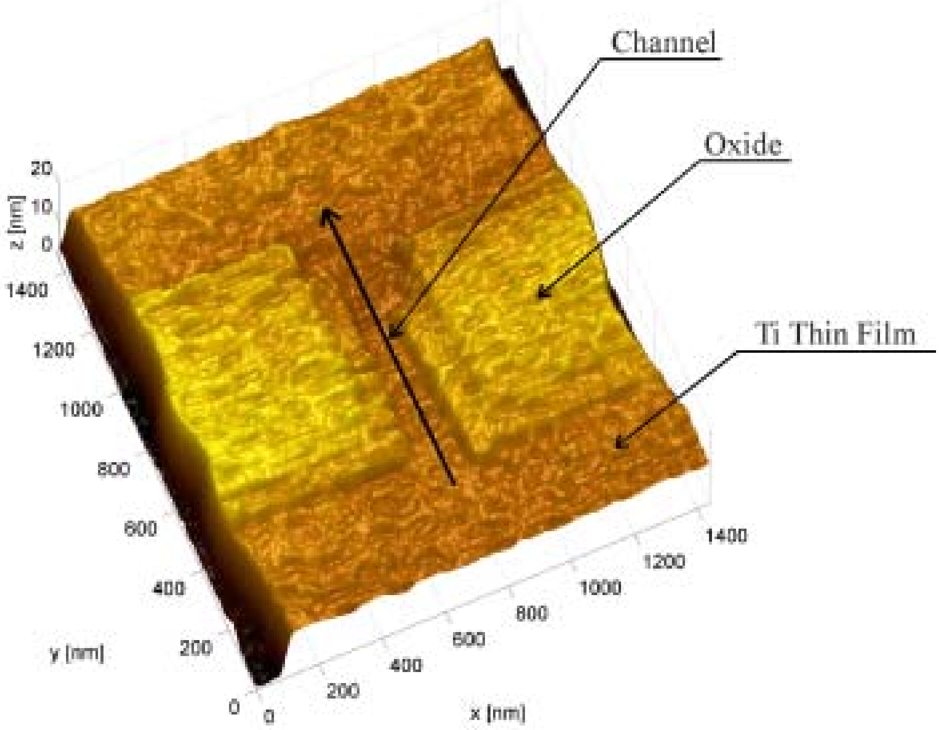

Fig. 9: A conduction gap made by AFM local anodic oxidation of the Ti line.

If the resistivity of the meander is continuously monitored during oxidation, its nonlinear increase with the gap narrowing should be observed. Making oxide lines across the gap, tunneling effects through the non-conducting barrier might be studied as well. Results of this work have been published in [18].

5 INVESTIGATIONS OF SI(111) SURFACES BY HIGH TEMPERATURE UHV STM

To acquire an experience in the application of scanning tunneling microscopy (STM) for a study of atomic surface structures, a series of experiments have been carried out using facilities at partner‘s universities abroad. At Arizona State University in Tempe (USA) in the group of Prof. I. S. T. Tsong individual phases of reconstructed Si(111) surfaces have been studied using an ultra-high vacuum STM with a high temperature capability. This part summarises the author's work that had been done during his 4-month stay in the year 2000.

5.1 INSTRUMENTATION

The high temperature ultra-high vacuum STM instrument designed and built by Mark Lamb as a part of his Ph.D. work [19]. The UHV chamber was pumped by combination on an ion pump and titanium sublimation pump. The base pressure of the vacuum system was in an order of 10^{-8} Pa. Using the titanium sublimation pump the ultimate pressure that was possible to reach was $2x10^{-9}$ Pa. The vibration isolation is one of the most important tasks for any high resolution imaging system, especially for the microscopes capable of providing atomic resolution. This system embedded a novel vibration isolation stage based on the passive magnetic levitation having its resonance frequency below 1 Hz.

In this instrument resistive heating by direct current passing through the silicon sample was used. The method was chosen due to the ability to modify the step growth process by the direction of the heating current. When the current flows in the step down direction it induces step bunching and wide terraces are created; when the opposite flow is used the terraces of smaller width are grown [20].

One of the disadvantages of the direct resistive heating is that heating power is subject to the sample-conductivity temperature dependence. This makes stable heating at lower temperatures difficult with the heating current being kept constant. Improved method of the controlling sample temperature is demonstrated in the following section.

5.2 HOT STM TEMPERATURE CONTROLLER

A standard technique for obtaining clean Si surfaces in ultra-high-vacuum (UHV) involves heating the sample close above 1200 °C for about 30 seconds total time [21]. The procedure is known as flashing the sample. At this temperature the native oxides are removed by their thermally initiated decomposition at the surface by which it is possible to obtain an atomically clean surface. Heating to such high temperatures introduces an extensive outgassing from the sample as well as from the surrounding surfaces being heated by the sample radiation. Therefore, the sample and the holder have been outgassed for several hours at the temperature about 700 °C prior to the main flashing procedure. Even then the outgassing at 1200 °C is high enough to disturb the UHV conditions significantly. As it is desirable to keep the chamber pressure below $1x10^{-7}$ Pa during the flashing, the procedure is usually divided into a sequence of short flashing (~1s) repeated about 30 times in order to obtain a total flashing time of 30 s.

At the beginning a manual method for the flashing had been utilized. This required the presence of an experienced operator and the reproducibility of the flashing conditions was poor. It was not possible to control the speed of cooling down the sample because this was only driven by the system thermal conductivity. Furthermore, it was desirable to keep the sample at about 500 °C for the period between the high temperature flashes in order to avoid a condensation from the worsened vacuum on its surface. It was not possible with this instrumental setup.

Our aim was to automatize the procedure and improve its repeatability as much as possible; a new hardware setup had been built in order to control the heating by means of a personal computer. In the design an input/output computer board was utilized. By means of an input channel it was possible to digitally read temperature from the pyrometer and by an analogue output to adjust the power supply current accordingly. Software for the heating control was developed by the author. It was named Hot STM Temperature Controller and it enables two regulation modes:

- Passive mode: a simple controlling of the heating current (I) and simultaneous monitoring and recording the sample temperature (T).
- Active mode: the heating current is adjusted to maintain the required temperature by means of a feedback loop regulator. There is an option to set the gains (P - proportional, I - integral, D - derivate parameters) in order to optimize the feedback loop speed for fast or slow regulation.

The passive mode was mainly used for the flashing procedure. During the flashing the current could not be controlled by the feedback loop as the process is very fast and it would require very fast loop response resulting in the regulation overshoots. Therefore a method of current profiling was implemented. The software controlled the heating current to match the current profile as much as possible and the temperature curve was passively recorded during this time.

The active mode was applied when long term-regulation at a fixed temperature was required or slow change from one temperature to another was needed. This allowed to keep the temperature constant for long, literally unlimited, time (e.g. during the sample degassing). The precision of the regulation was better than 1 °C.

The flashing procedure controlled by this software was tested using the sample that was cut out of a P-doped Si(111) wafer. After its heating up to a maximum of approximately 1240 °C the sample was radiation quenched by lowering the current. In Figure 10 three heating current profiles and corresponding sample temperature curves are shown. Since the beginning of the phase transition from the high-temperature 1×1 metastable phase to the low-temperature 7×7 thermodynamically stable reconstruction is believed to occur between 830-870 °C [22] the curves are labelled by the liner approximation of the decay rate in this range.

The fastest quench of 320 °C/s simulates the manual flashing by switching off the heating suddenly. In the second profile the current decrease is slowed down and its target value is 0.46 A which results in a slower temperature decrease of 240 °C/s and the sample temperature is maintained at approximately 500 °C between the single flashes. Using both 240 and 320 °C/s temperature curves resulted in a quite highly disordered silicon surface with the large areas of trapped 1×1 reconstruction [19].

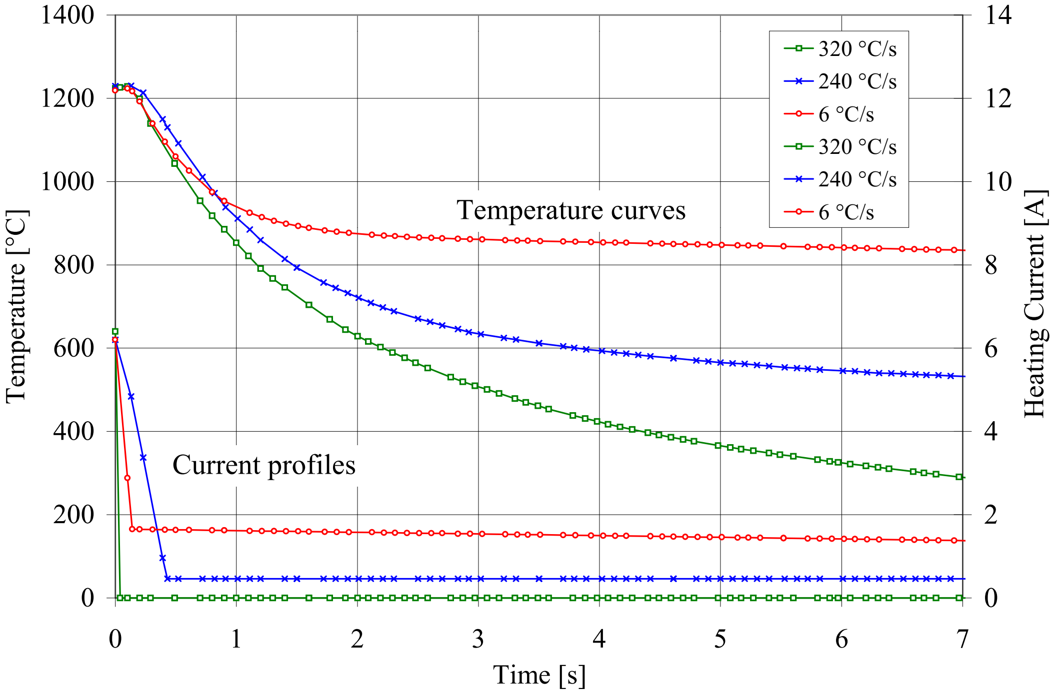

Fig. 10: Sample temperature curves measured for three current profiles.

Best results were obtained for the third current profile characterised by a rapid current decrease to 1.65 A followed by a very slow descent of 0.04 A/s to the final value of 0.46 A. The quenching speed for this current profile was ~6 °C/s. We have used the fast (240 °C/s) quenching for repeated flashing to accumulate total of 30 seconds above 1200 °C. However, the last 2 or 3 flashing cycles were done using the very slow quenching speed. The samples processed using the technique showed perfect regularity of the 7×7 reconstruction with the six-fold rotational symmetry.

The software regulation had proved reliable and was used routinely for long-term temperature regulation as well as for the flashing. It made heating of the samples more accurate, reproducible and at last but not least more comfortable.

5.3 TIP-INDUCED NANOSTRUCTURES ON SI(111) 7×7 SURFACE

Similar to the AFM technique the scanning tunneling microscopy is used not only for monitoring the surfaces but it can be the powerful tool for a local modification of the surface structure, i.e. fabrication of the nanostructures. It has been found that various nanostructures (islands) on silicon surfaces might be generated by controlled approaching or retracting the tip above the surface [23]. The high temperature STM has ability to study the structures at elevated temperatures at which the structures are thermodynamically unstable and tend to decay in time. The observation of decay process can give information about fundamental diffusion processes on surfaces. In this study the attempts were made to grow silicon islands or produce craters on the Si(111) 7x7 surface and to observe their decaying.

The wide terraces are required in order the island can be grown far from the steps. In that way the step effect on the island decaying is avoided. One of the parameters that significantly influence the terraces width is a miscut angle of a silicon wafer, therefore a p-type Si(111) with a very small miscut angle of 0.1° was used. The width of the terraces is furthermore enhanced by direct current heating in the step up direction that causes the step bunching induced by the electromigration [20]. The terrace width was bigger than 500 nm with fairly uniform distribution over the sample area.

First recipe for making the nanostructures with an STM tip was acquired from the correspondence with Mr. Kazuhiko Hayashi [23]. Using this method we succeeded in making the islands couple of times, however most of time it was not possible to make them. The problem with producing the islands could be explained by lack of the Si material on the STM tip that could be transferred on the surface and create the island. Therefore, we proposed the following modification of the method based on the experience from our experimental efforts. In this method the sample is prepared by the flashing followed by fast quenching (240 °C/s) to produce a highly disordered surface. At temperature above 500 °C the regions with the areas of trapped 1 × 1 or disordered clusters are found. The sample bias of approximately 10 V is applied until the surface begins to show signs of cluster and/or vacancy island formation and/or movement, sometimes losing atomic resolution. Alternatively, the bias is set to 0 V for a few seconds or switched from a positive to negative value several times. This causes the tip to touch the surface and possibly to pick up some material. Then a normal sample bias voltage is restored and the region is scanned repeatedly until atomic resolution is recovered. The idea was to use more thermodynamically unstable surface that can more easily release some material, therefore make it easier to pick up the material on the tip.

The tip is retracted far from the surface while the sample is flashed again followed by slow quenching 6 °C/s to obtain the perfect 7 × 7 reconstruction. After the tip is brought back to the tunneling contact and quality of the 7 × 7 reconstruction is checked the production of islands/craters might begin. In order to produce the silicon islands, the sample bias is set close to 0 V for approximately 1 minute. This modified method did not work always as well, but was a bit more successful than the previous method.

In Figure 11 a hillock (pyramidal) island imbedded in a crater was made at a temperature of 520 °C using the modified method. The volume of the material within the hillock was much bigger than the volume missing in the crater proving that the material transfer from other areas must be involved in the hillock formation as well. As the time was too short (<1 minute) to form the hillock from the atoms diffusing on the surface, we believed that Si atoms were dropped into the crater from the STM tip during their physical contact.

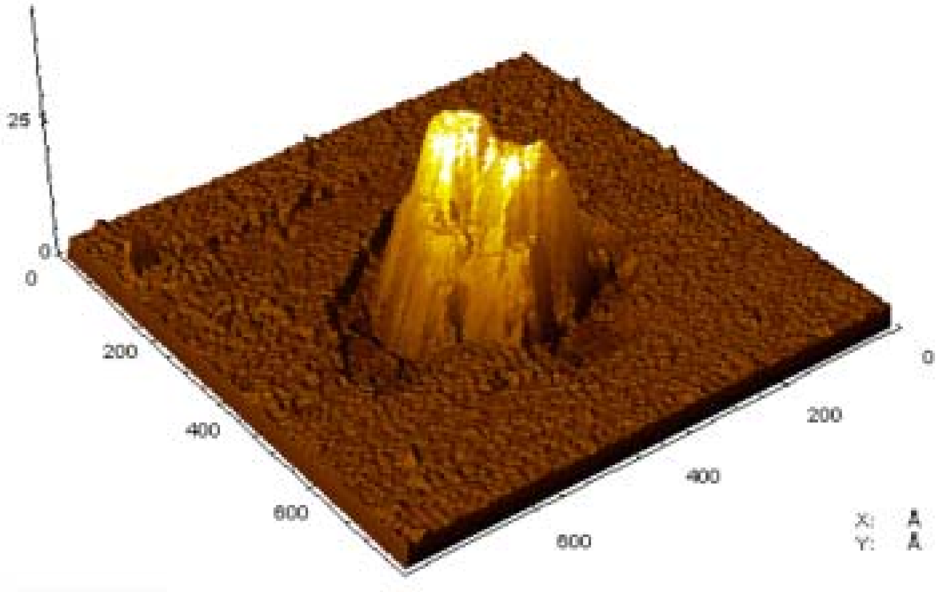

Fig. 11: Tip-induced hillock imbedded into a crater at temperature 520 °C.

In the case there is not enough material on the tip to produce an island the tip can still modify the Si(111) 7 × 7 reconstructed surface. The craters could be created when the sample bias is changed from 2 V to –2 V over a period of about ten seconds at the tunneling current greater than 1 nA. This causes the tip to physically touch or bury into the surface and destruct its structure. It was observed that such a crater decays in time until it fully disappears. It is believed that it is filled with atoms diffusing along the surface due to the elevated temperature and their electromigration, though the exact mechanism is yet not fully understood [24].

A crater was made by the STM tip at a temperature of 520 °C. It was observed that the crater is preferentially being filled from the corner that was close to the cathode side of the sample. The anisotropic decaying was related to the direction of the heating current and was in agreement with observations described in [24]. The separate clusters of atoms, so called magic clusters, seemed to particularly accumulate in the bottom-left corner as well. However there are several magic clusters seen close to the top-left edge as well, so it was impossible to confirm the same behaviour as in [24].

The whole sequence of decaying of another tip-induced crater was recorded at 512 °C until the crater fully disappeared. Fig. 12 shows the number of the crater vacancies as a function of time. It is apparent that the decay curve drops down faster when the crater becomes smaller. This behaviour was observed at least two times on bigger craters. Furthermore, it was observed that when a very small crater was created it decayed so fast that it was not possible to closely watch the process at all. The decay curve was fitted with two linear dependencies showing the decay rate of approximately 0.7 atoms/s at the beginning and much higher rate of 3.6 atoms/s at the end of decay. This indicates that there is discontinuity at the end of the decay.

Although the direction of the heating current is the same for the previous crater, it seemed that this crater is being filled in the direction perpendicular to the heating current. Moreover, many magic clusters can be seen on the opposite side. This is in contradiction with the results presented in [24]. In our experiment the specific resistivity of the sample was 0.1 Ω cm (contrary to 0.05 and 0.01 Ω cm) and there might be different thermal conductivity from the sample to the sample holder. Both differences lower the heating current needed to obtain the temperature about 500 °C, therefore, the current density is lowered and influence of the electromigration might become insignificant.

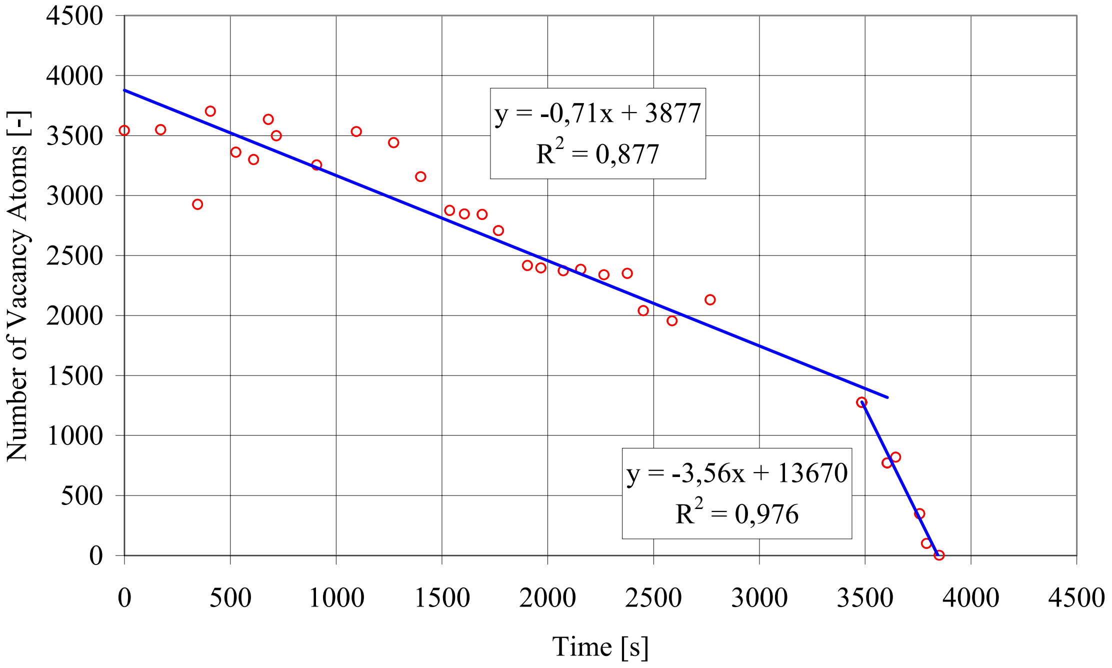

Fig. 12: Number of vacancies in the tip induced crater as a function of time.

However, it should be considered that other mechanism could be involved in the crater decay. Such mechanism might be e.g. filling the crater by atoms deposited on the tip and dropping off the tip introducing significant disturbance to the decay process by observing the process with the STM technique. It must be point out that due to the difficulties with fabrication the nanostructures only the low number of craters/islands was produced and this study therefore lacks adequate quantification necessary for this kind of the experiment.

6 DEVELOPMENT OF THE SECONDARY ELECTRON DETECTOR FOR LOW VACUUM SCANNING ELECTRON MICROSCOPY

In the last more than 50 years the scanning electron microscopy (SEM) have become a routine tool for observing the surface of the conductive specimens or specimens that are coated by a conductive layer. The wet (biological) or volatile compounds containing specimens could not a subject of observation in their native state due to the high vacuum in the specimen chamber (typically 10^{-3} Pa) causing their dehydration, hence a special and difficult specimen preparation was necessary to carry out. Furthermore non-conductive specimens could not be imaged properly due to their surface charging by the interaction with an electron beam [25]. Therefore their surface must be coated with conductive layer that might result in the overlaying and hiding of their fine structure, the structure one wants to see.

From these reasons a new technique of the scanning electron microscopy have been developed – it is called variable pressure or environmental SEM. The technique is based on the differentially pumped system where an electron optical column is maintained under the high vacuum conditions substantial for its operation. Contrary to that a specimen chamber is kept at much higher pressure (typically 1 to 2000 Pa). The dehydration of the wet specimens is significantly slowed down under these pressures. Furthermore, the imaging of the nonconductive specimens becomes possible thanks to the charge compensation by the positive ions originating from the electron-gas interaction. The samples can be observed in their native, uncoated state.

A detection of the backscattered electrons under low vacuum does not present a problem – the same detector as for the high vacuum can be used. Contrary to that the standard high vacuum secondary electron detector can not be used under such conditions due to the reasons described hereafter. A special low vacuum secondary electron detector must be used.

This chapter describes a work that has been done in the company TESCAN, s.r.o., the world-wide-recognized producer of the scanning electron microscopes [3]. The author, employed by the company, has taken part in the development of a new method to detect secondary electrons under low vacuum condition. The methods of the SE detection through ionisation of gas molecules in the specimen surroundings have been protected by patents [26, 27], therefore the development of the new SE detector was necessary.

6.1 PRINCIPLES OF THE DETECTOR OPERATION

The conventional Everhart-Thornley secondary electron detector embodies a high voltage of order of a few kilovolts at the scintillator [28]. It can not be used in a low vacuum environment due to the fact that such high voltage causes catastrophic discharge breakdown between the scintillator and grounded walls of the system (due to minimum in the Pashen curve). Tescan company has a wealth of experience in the design of Everhart-Thornley SE detectors for high vacuum environments. Thus we have focused our efforts on the detection of SE by means of modified E-T detector.

The modified design consists of a differentially pumped detection chamber separated from the specimen chamber by a microlens differential barrier and pumped by means of a small turbomolecular pump. The microlens differential barrier is a special metallic disc with a number of small holes. It serves as a set of apertures for differential pumping and at the same time creates an array of microlenses focusing the secondary electrons into the holes and transporting them towards a detector scintillator. The detector was named Low Vacuum Secondary Tescan Detector, thus the abbreviation LVSTD is used widely in the following text.

Figure 13 shows a scheme of the LVSTD detector. The detector works as follows: The primary electron beam 1 accelerated in the electron-optical column strikes the surface of a specimen 2 located in the specimen chamber 3. The impinging electrons cause the emission of the secondary electrons, the energy of the emitted electrons being only a few electronvolts, the energy distribution peaks at 2-5 eV [25]. The secondary electrons, in view of their low energy, are strongly attracted by the electric field of the hemispherical input grid 4 that is biased to approximately +150 V DC. As the grid is made of the thin wires most of the electrons passes through and is furthermore attracted by the microlens differential barrier 5 biased to +500 V. The scintillator 6 coated by a conductive layer 7 biased to +10 kV is located right behind the barrier in the detector chamber 8. The electric field created by the high potential on the scintillator layer penetrates through the holes of the barrier and works as the electrostatic lenses focusing electrons into the holes. The electrons that cannot be fully focused and impinge upon the barrier surface between the holes cause secondary emission from the disc creating “tertiary” electrons, some of them are subsequently transported into the detection chamber through the microlens array. In this way they contribute to the useful signal.

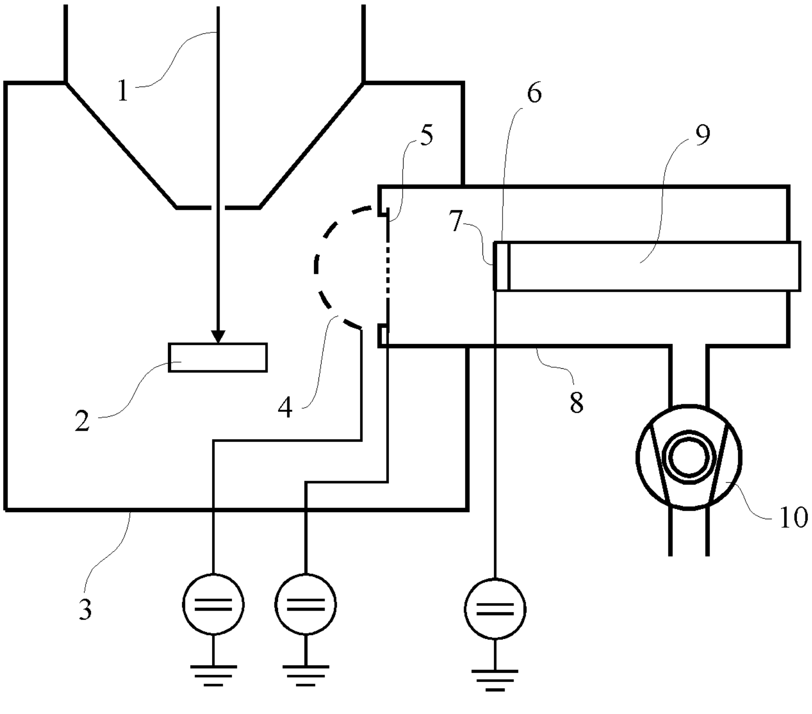

Fig. 13: Schematic view of the LVSTD detector.

As it is known in the art, due to the voltage of 10 kV and a small thickness of conductive layer 7 (in order few tens of nanometres), the secondary electrons pass through the coating and strike the scintillator with energy of close to the original energy of 10 keV. The light produced by the scintillation of the electrons is then transmitted through a light guide 9 to a photo-multiplier (not shown), giving an electric signal at its output.

The design of the differential barrier (number, shape and area of the holes) is optimized in order to achieve maximum transmittance for the secondary electrons while maintaining its vacuum conductivity sufficiently low. With our current design it is possible to operate the detector up to pressure of 500 Pa in the specimen chamber. Up to this limit the turbomolecular pump 10 is capable to keep the detector chamber pressure below approximately 5 Pa that is sufficient for discharge-free detector operation.

6.2 DETECTOR PERFORMANCE TESTS

A number of different nonconductive or biological samples have been observed in order to evaluate the performance of the LVSTD detector in comparison with the backscattered electron detector. All experiments have been performed using standard TESCAN Vega 5136MM microscope (with the low vacuum capability) equipped with the LVSTD detector [3].

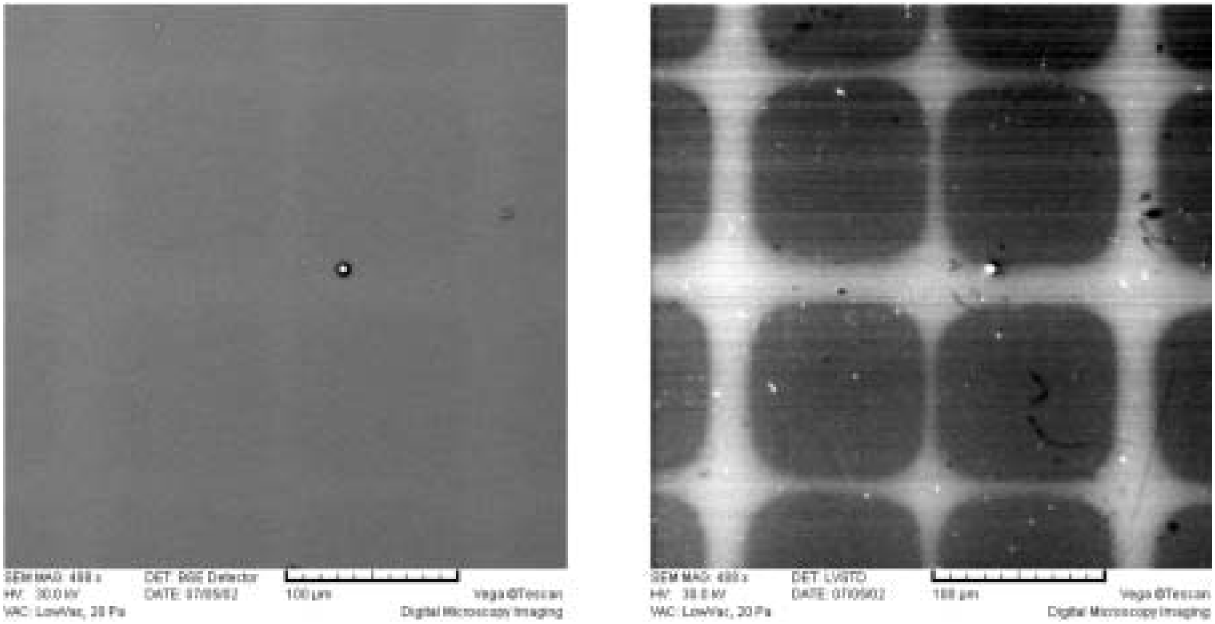

Fig. 14: Silicon substrate covered by the carbon thin film patterned into squares, standard backscattered (left) and LVSTD secondary (right) electron image.

The ability to detect secondary electrons preferentially to backscattered electrons is an important feature of any SE detector. The clear difference in image contrast and details could be seen in all images recorded with the LVSTD. However, to confirm that the signal is predominantly from secondary electrons a special sample was made of a silicon substrate on which a carbon square pattern was deposited (≈3nm thick). Although the surface of the sample is very flat (showing no topographic contrast) it is possible to distinguish between the areas of Si and C due to the difference in the secondary emission yield of Si and C (0.08 and 0.05 for Si and C respectively, for the primary beam energy 30 kV), Figure. 14 right. This is due to the fact that the secondary electrons originate from the top layers of the solid sample giving the true surface resolution and contrast. Contrary to that, the backscattered electrons originate from much bigger volume, therefore from bigger depth, and BE signal is mainly provided by the Si substrate and only insignificantly influenced by the thin layer of C, Figure. 14 left.

Another important parameter of any SEM detector is its frequency bandwidth. In the case that this bandwidth is lower than the frequency of the scanning an image becomes blurred in the direction of the fast scanning. The conventional E-T detector has its maximum bandwidth in order of several MHz [25]. In Figure 15 two line-scans across a sharp edge of a test grid are compared for a standard E-T detector and LVSTD detector. The pixel-to-pixel time was 600ns resulting in the frequency of approximately 1.7 MHz. Both detectors show the similar timing resolution.

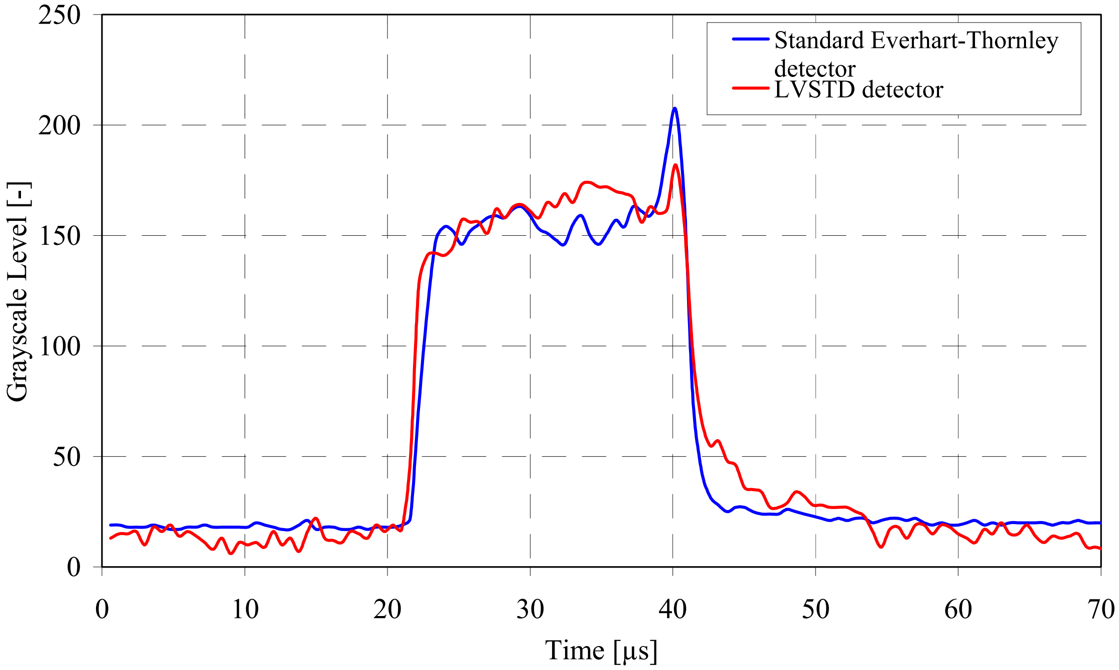

Fig. 15: Fast linescan across the test grid confirms the similar timing response of the LVSTD detector in comparison with the conventional E-T detector.

6.3 RESULTS

The modified design of the E-T detector, with a separated and differentially pumped detection chamber, has been completed and tested. The detector is nowadays commercially available under the trade name Low Vacuum Secondary Tescan Detector - LVSTD for all Tescan variable pressure scanning electron microscopes. As the detector design includes a considerably inventive step the international patent application has been filled [29]. Some aspects of the detector design and operation have been published in [30].

The original solution of the LVSTD allows to obtain the following most important and unique features:

- True topographic contrast can be imaged under the low vacuum conditions thanks to the detection of real slow secondary electrons.
- The fast response time of the detector allows fast scanning speeds.
- The image contrast and shadowing is very close to the high vacuum SE detectors.

7 CONCLUSIONS

This work has demonstrated the basic principles of atomic force microscopy and scanning tunneling microscopy, as well as some particular design aspects and applications of the UHV STM/AFM instrument. The instrument including the new optical detection unit has been designed, built and tested. The precision of the instrument measurements was calibrated. The error of the measurement was less than ±1% of the measured distance/height. Its ability of high resolution, even atomic resolution, three-dimensional imaging of solid surfaces was proved.

The AFM and STM technique has been applied in many surface studies. In this thesis the applications for the morphology analysis of thin films and microstructures produced by ion beam technology were presented. The microscopy images helped us to optimize technological parameters in order to obtain the required results.

Furthermore, the home-built AFM/STM instrument proved to be a useful tool for the fabrication and testing of titanium oxide nanostructures. It was shown that the height of Ti oxide lines increases linearly with the voltage between a tip and a sample. The half-width of the lines do not depend linearly on this voltage. Very complex patterns can be made by using this AFM instrument and its software extension, hence, local anodic oxidation can be used for a study of quantum effects in nanostructures and for experiments in fabrication of nanoelectronic devices, e.g. single electron transistors.

During the stay at the partners's university the experience with the high temperature ultra-high vacuum STM technique was gained and new instrumentation and software was developed. The work demonstrated the ability of STM atomic resolution imaging and showed some basic principles of producing and analyzing the nanostructures at the atomic level.

At the last part of the Ph.D. study the author aimed his effort to the field of scanning electron microscopy, an alternative and complementary technique that is also dealing with characterization of the surfaces at micrometer and nanometre scale. He took a part in developing a novel secondary electron detector for low vacuum conditions in the company TESCAN, s.r.o. This development was successfully completed and the international patent application was filled. Nowadays the author is employed as a project leader in the company and continues development in the field of applied physics, i.e. development of the scientific instruments.

The development of any scientific instrument requires a lot of experience as well as open minds and attitudes for the innovative solutions, a strong will to get results and much more patience until getting them. The author wishes to the people continuing this work to have enough of all.

8 REFERENCES

[1] G. Binning, H. Rohrer, Ch. Gerber, E. Weibel: Surface Studies by Scanning Tunneling Microscopy, *Physical Review Letters*, 1982, no. 49, p. 57-61.

[2] G. Binning, C. F. Quate, Ch. Gerber: Atomic Force Microscope, *Physical Review Letters*, 1986, no. 56, p. 930-933.

[3] TESCAN, s.r.o.: Home page [online], last revision 4.5.2005 [cited 10.5.2005], www.tescan.cz.

[4] MikroMasch: Silicon Home page [online], last revision 23.2.2005 [cited 15.3.2005], www.mikromasch.com.

[5] R. Kalousek, F. Lopour, P. Dub, T. Šikola: Physical principles and resolution limits of the noncontact AFM mode – simulation of cantilever oscillations (in Czech), *Československý časopis pro fyziku*, 2001, no. 1, p. 43-48.

[6] F. Lopour: Design of the STM/SFM instrument for a monitoring of solid surfaces under UHV conditions (in Czech), diploma work, *ÚFI FSI VUT Brno (Brno University of Technology, FME, IPE)*, 1997, p. 23-43.

[7] F. Lopour, R. Kalousek, D. Škoda, T. Šikola: Design and application of an UHV SPM (in Czech), *Jemná mechanika a optika*, 2001, no. 4, p. 133-135.

[8] L. Howald, H. Rudin, H. J. Güntherodt: Piezoelectric inertial stepping motor with spherical rotor, *Review of Scientific Instruments*, 1992, vol. 63, no. 8, p. 3909-3912.

[9] Physik Instrumente GmbH & Co. KG: Piezo Engineering, Nano-Positioning [online], last revision unknown [cited 8.4.2005], www.physikinstrumente.de.

[10] F. Matějka, J. Matějková, F. Lopour: Possibilities of testing the metric of STM and AFM instruments (in Czech), *Československý časopis pro fyziku*, 2001, no. 1, p. 38-42.

[11] D. Škoda: Development and testing of the UHV-compatible microscope AFM/STM (in Czech), diploma work, *ÚFI FSI VUT Brno*, 2001, p. 20-28.

[12] S. Hembacher, Franz J. Giessibl, Jochen Mannhart, and Calvin F. Quate Revealing the hidden atom in graphite by low-temperature atomic force microscopy, *Proceedings of the National Academy of Sciences of USA*, 2003, vol. 100, no. 22, p. 12539-12542.

[13] T. Šikola, J. Spousta, R. Češka, J. Zlámal, L. Dittrichová, A. Nebojsa, K. Navrátil, D. Rafaja, J. Zemek, V. Peřina: Deposition of Metal Nitrides by IBAD, *Surface and Coatings Technology.*, 1998, nos. 108–109, p. 284-291.

[14] F. Lopour, P. Bábor, T. Šikola, J. Spousta, L. Dittrichová, F. Matějka, J. C. C. Duarte: Etching of Microstructures and Modification of Solid Surfaces by Low Energy Ion Beams, *Proceedings of the 3rd International Conference MicroMat 2000*, editors B. Michel, T. Winkler, M. Werner, H. Fecht, 2000, p. 919-922.

[15] D. Stievenard, P. A. Fontaine, E. Dubois: Nanooxidation using a scanning probe microscope: An analytical model based on field induced oxidation, *Applied Physics Letters*, 1997, vol. 70, no. 24, p. 3272-3274.

[16] R. J. M. Vullers, M. Ahlskog, M. Cannaerts, C. J. Van Haesendonck: Field induced local oxidation of Ti and Ti/Au structures by an AFM with diamond coated tips, *Journal of Vacuum Science and Technology B*, 1999, vol. 17, no. 6, p. 2417-2420.

[17] K. Matsumoto, M. Ishii, K. Segawa, Y. Oka: Room temperature operation of a single electron transistor made by the scanning tunneling microscope nanooxidation process for the TiO_x/Ti system, *Applied Physics Letters*, 1996, vol. 68, no. 1, p. 34-36.

[18] F. Lopour, R. Kalousek, D. Škoda, J. Spousta, F. Matějka, T. Šikola: Application of AFM in Microscopy and in Fabrication of Micro/Nanostructures, *Surface and Interface Analysis*, 2002, vol. 34, no. 1, p. 352-355.

[19] M. Lamb: Scanning A novel high temperature scanning tunneling microscope for investigating semiconductor surfaces, Ph.D. Thesis, *Department of Physics, University of Houston*, 2001.

[20] Y. N. Yang, E. S. Fu, E. D. Williams: An STM study of current-induced step bunching on Si(111), *Surface Science*, 1996, no. 356, p. 101.

[21] J. A. Kubby, J. J. Boland: Scanning tunneling microscopy of semiconductor surfaces, *Surface Science Reports*, 1996, no. 26, p. 61-204.

[22] S. Kitamura, T. Sato, M. Iwatsuki: Observation of surface reconstruction on silicon above 800 °C using the STM, *Nature*, 1991, no. 351, p. 215-217.

[23] A. Ichimiya, Y. Tanaka, K. Hayashi: Relaxation of Nanostructures on the Si(111)(7×7) Surface by High Temperature Scanning Tunneling Microscopy, *Surface Review and Letters*, 1998, vol. 5, nos. 3-4, p. 821-832.

[24] M. S. Ho, I. S. Hwang, T. T. Tsong: Direct observation of electromigration of Si clusters on Si(111) surfaces, *Physical Review Letters*, 2000, vol. 84, no. 25, p. 5792-5795.

[25] L. Reimer: Scanning Electron Microscopy, *Springer-Verlag Berlin Heidelberg*, 2nd edition, 1998, p. 10, 316-320, 7-8.

[26] J. F. Mancuso et al.: Secondary Electron Detector for Use in Gaseous Atmosphere, *United State Patent*, Patent Number 4,785,182, 1988.

[27] P. Sudraud et al., LEO Electron Microscopy Limited: Scanning Electron Microscope, *United State Patent*, Patent Number 6,365,898, 2002.

[28] T. E. Everhart, R. F. M. Thornley: Wide-band detector for micro-microampere low-energy electron currents, *Journal of Scientific Instruments*, 1960, no. 37, p. 246-248.

[29] Tescan, s.r.o. (applicant), M. Jacka, M. Zadražil, F. Lopour (inventors): Secondary electron detector, international patent application, *World Intellectual Property Organization*, international publication no. WO 2004/059691, 2004.

[30] M. Jacka, M. Zadražil, F. Lopour: A Differentially Pumped Secondary Electron Detector for Low Vacuum Scanning Electron Microscopy, *Scanning*, 2003, vol. 25, p. 243-246.

AUTHOR'S CURRICULUM VITAE

Personal data:

Name:	Filip Lopour
e-mail:	filip.lopour@tescan.cz
Date of Birth:	April 17th 1972
Nationality:	Czech

Education:

1997- Ph.D. study in the field of Physical and Materials Engineering at the Brno University of Technology, Faculty of Mechanical Engineering, Institute of Physical Engineering.

1990-97 Master degree study in the field of Physical Engineering at the Brno University of Technology, Faculty of Mechanical Engineering, Institute of Physical Engineering, focused on the applied physics (e.g. particle optics, physics of the surfaces and thin films, light optics and fine mechanics), Diploma work: Design of an STM/SFM instrument for the monitoring of solid surfaces under UHV conditions.

1986-90 Secondary Technical School of Mechanical Engineering, Sokolská 1, Brno, 4-year study, specialisation: technology in mechanical engineering.

Job experiences:

2001- TESCAN, s.r.o., Brno – producer of the Scanning Electron Microscopes, position: deputy manager of the Research and Development department, project leader responsible for the development of the physical parts of the microscopes (applied physics).

Study periods abroad:

1994 University of Salford, Great Britain (6 months), contribution to the project: Design of the UHV parts for novel Dual low energy ion beam deposition system.

2000 Arizona State University, Tempe, USA (4 months), active contribution to the project: Development and application of a high temperature ultra-high vacuum STM.

Brno May 27th 2005 Filip Lopour

ABSTRAKT

Převážná část této disertační práce se zabývá technikami rastrovací tunelové mikroskopie (Scanning Tunneling Microscopy – STM) a mikroskopie atomárních sil (Atomic Force Microscopy - AFM), souhrnně označovaných mikroskopie rastrovací sondou (Scanning Probe Microscopy - SPM).

Práce popisuje některé aspekty konstrukce ultra-vakuově kompatibilního mikroskopu SPM vyvinutého a vyrobeného na Ústavu fyzikálního inženýrství Fakulty strojního inženýrství VUT v Brně. Zejména je zde pojednáno o návrhu nové optické jednotky detekce průhybu raménka pro metodu AFM, zahrnující vývoj speciálních manipulátorů pro natáčení zrcadel na bázi inerciálního piezokeramického pohonu. Je zde rozebrána otázka testování přesnosti skeneru a možnosti kalibrace tohoto mikro-/nano-manipulátoru za účelem dosažení vyšší přesnosti měření. Dále je zde demonstrována schopnost přístroje k dosažení atomárního rozlišení na vysoce orientovaném pyrolitickém grafitu v režimu STM.

Další část práce popisuje aplikaci mikroskopie AFM pro monitorování tenkých vrstev a mikrostruktur vytvořených depozicí a leptáním iontovými svazky. Následně je ukázána možnost nejen zobrazování, ale přímo vytváření struktur nanometrických rozměrů pomocí mikroskopie atomárních sil, tzv. nanotechnologie. V tomto případě se jedná se o lokální anodickou oxidaci tenkých vrstev titanu a možnosti vytváření nanostruktur pro studium kvantových efektů.

Podobně je tomu také v další kapitole, která popisuje aplikaci vysokoteplotního ultra-vakuového mikroskopu STM pro vytváření a sledování struktur atomárních rozměrů. V jedné z aplikací byla pozorována rekonstrukce Si(111) 7×7 na úrovni atomárního rozlišení a následně byly na povrchu vytvářeny „ostrůvky“ nebo „krátery“ rozměrů řádu jednotek až desítek nanometrů a sledován jejich rozpad s časem.

Poslední část je zaměřena na poněkud odlišnou oblast - techniku rastrovací elektronové mikroskopie a pojednává o vývoji detektoru sekundárních elektronů pro detekci v režimu nízkého vakua v komoře preparátu, v oblasti jednotek až stovek Pa. Tento detektor nachází široké uplatnění při pozorování nevodivých, případně vlhkých preparátů a umožňuje kvalitní zobrazení topografie těchto povrchů v nativním stavu bez nutnosti jejich náročných a často destruktivních úprav.